Electronic Supplementary Material (ESI) for Journal of Materials Chemistry A.
This journal is © The Royal Society of Chemistry 2023

Exploiting Grain Boundary Diffusion to Minimize Dendrite Formation in Lithium Metal-Solid State Batteries

Jeong Seop Yoon[a], Hafeez Sulaimon[a], Donald J. Siegel[a,b]

[a] Department of Mechanical Engineering, University of Michigan, 2350 Hayward Avenue, Ann Arbor, Michigan 48109, United States

[b] Walker Department of Mechanical Engineering, Texas Materials Institute, Oden Institute for Computational Engineering and Sciences, Joint Center for Energy Storage Research, University of Texas at Austin

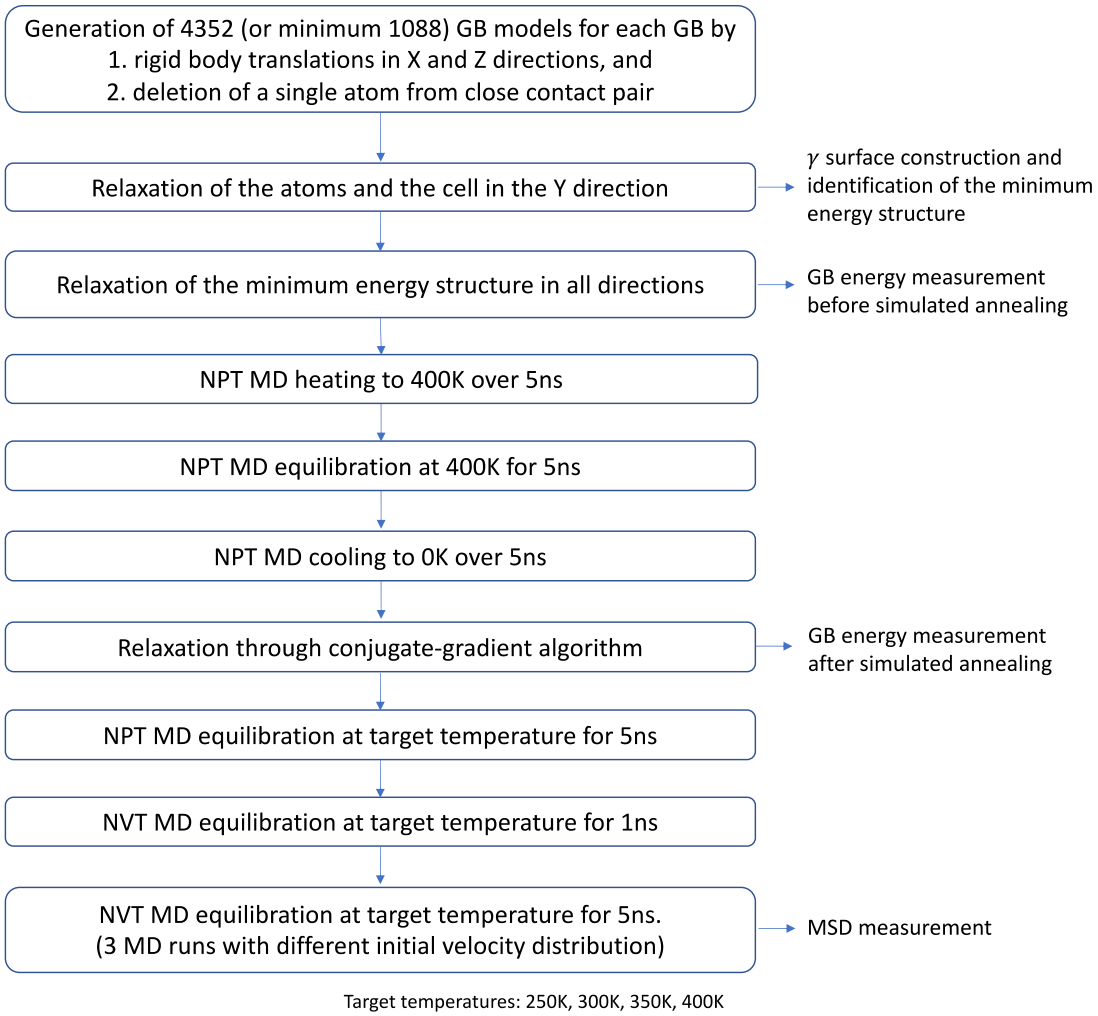

Figure S1. Flow chart describing the procedure for calculating GB diffusivity.

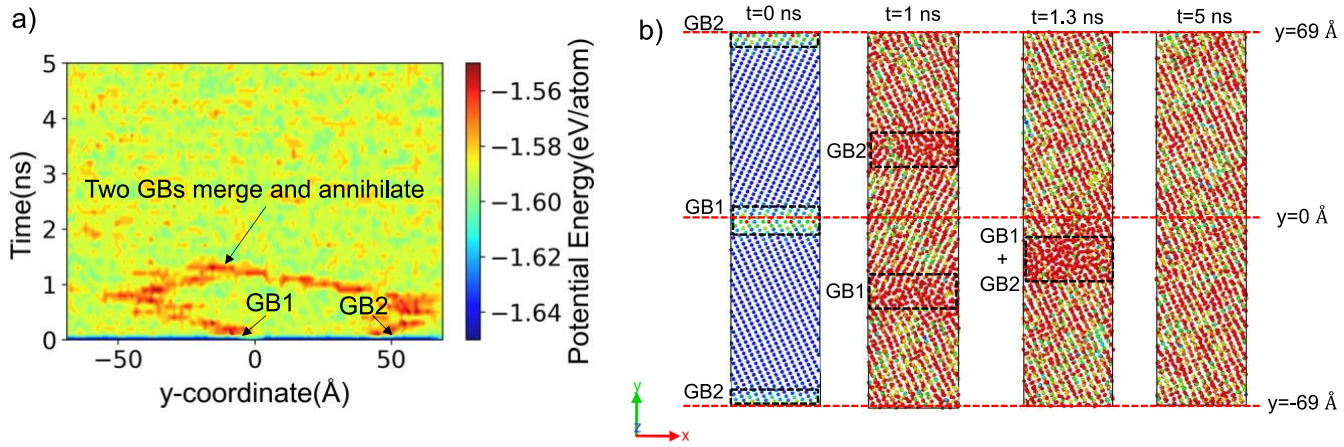

Figure S2. Migration of two $\Sigma 11(311)$/[01-1] tilt GBs and their subsequent annihilation during NPT annealing at 400 K. a) Color map showing the GB locations vs time based on the atomic potential energies. b) Snapshots during NPT annealing at selected times. Red indicates high potential energy and blue represents low potential energy.

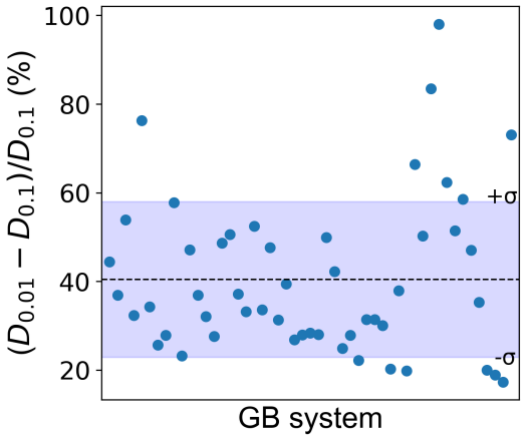

Figure S3. Change in calculated diffusivity when the identity of GB atoms are updated every 0.01 ns instead of every 0.1 ns. On average, GB diffusivity increases by 40% when the more frequent sampling rate of 0.01 ns is used. As a result, 0.1ns sampling rate is chosen since it does not alter conclusions of the current study and computational cost is less expensive.

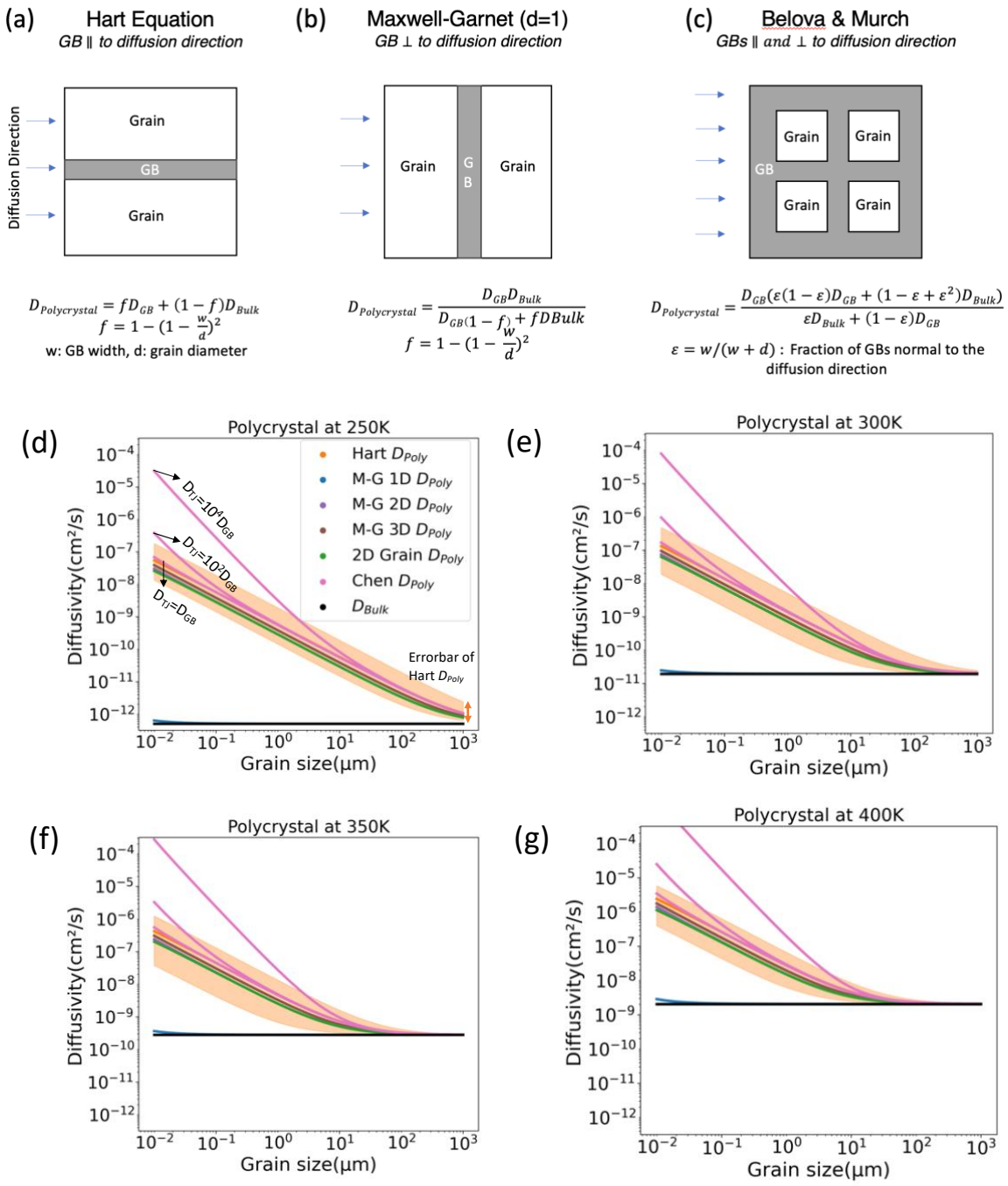

Figure S4. Polycrystalline diffusivity as predicted by 3 models that make different assumptions about GB orientation. Schematic a-c show the Hart model (GB parallel with 1-D diffusion), Maxwell-Garnet model (GB normal to 1-D diffusion), Belova & Murch 2D grain model (relative to 1-D diffusion, both normal and parallel GBs are present) respectively. Schematic d-g display Li Polycrystalline diffusivity as predicted by 4 models that make different assumptions about GB orientation. The Hart model, Maxwell-Garnet models, 2D grain model, and Chen's model are used to predict the polycrystalline diffusivity at (d) 250K, (e) 300K, (f) 350K, and (g) 400K, respectively. The calculation results of the Hart model are shown with the orange line, those of the Maxwell-Garnet models are shown with blue, purple, brown lines, the Generic 2D grain model with a green line, and the Chen model with pink lines. 3 different pink lines correspond to different assumptions on the triple-junction diffusivity. The orange shaded area represents the range of polycrystalline diffusivities from the Hart model, assuming scenarios where the largest and smallest GB diffusivities are used, respectively, as inputs to that model.

The Hart equation[1,2] for predicting polycrystalline diffusivity, $D_{polycrystal}$, assumes that the 1-D diffusion direction is parallel to the GB planes (Fig S4a). $D_{polycrystal}$ is calculated use the equation below, where f is GB volume fraction and D_{GB} and D_{Bulk} are the self-diffusivity of the GB and Bulk, respectively.

$$D_{Polycrystal} = fD_{GB} + (1-f)D_{Bulk}$$

$$f = 1-(1-\frac{w}{d})^2 \text{ (w: GB width, d: Grain diameter)}$$

In the 1-D Maxwell-Garnet model[2,3] the diffusion direction is normal to GB planes (Fig S4b). The model was derived to predict the diffusivity of a composite, where spherical inclusions and the matrix represent grains and GBs in a polycrystal, respectively.[4] The Maxwell-Garnet formula for $D_{polycrystal}$ is given by:

$$D_{Polycrystal} = \frac{D_{GB}[(f+d'-fd')D_{Bulk}+fD_{GB}(d'-1)]}{D_{GB}(d'-f)+fD_{Bulk}}$$

where d' is the space dimension (d'=1: GBs perpendicular to the diffusion direction, d'=2 or 3: GBs enclosing 2D-circular or 3D-spherical grains).

The 2D-patterned Grain model of Belova and Murch[2] falls between the extremes of the two previous models, in that it assumes that half of the GB planes are oriented perpendicular to the diffusion direction, while the other half are parallel (Fig S4c). In this case $D_{polycrystal}$ is given by:

$$D_{Polycrystal} = \frac{D_{GB}(\varepsilon(1-\varepsilon)D_{GB} + (1-\varepsilon+\varepsilon^2)D_{Bulk})}{\varepsilon D_{Bulk} + (1-\varepsilon)D_{GB}}$$

$$\varepsilon = w/(w+d)$$

where ε is the volume fraction of GBs normal to the diffusion direction.

Lastly, another polycrystalline diffusivity model proposed by Chen and Schuh[5] is examined. The assumptions in this model include: 1) bulk grains are enclosed by GBs and triple junctions (TJs), 2) TJs isolate the neighboring GB facets, 3) grain shapes are modelled as Voronoi polyhedral with a log-normal size distribution, and 4) no dislocation pipes are present in bulk grains. In this model, $D_{polycrystal}$ can be expressed as,

$$D_{Polycrystal} = f_{TJ}D_{TJ} + f_{GB}D_{GB} + f_{Bulk}D_{Bulk} + \frac{f_{TJ}f_{GB}(D_{TJ}-D_{GB})^2}{f_{TJ}(D_{TJ}-D_{GB})-2(f_{GB}+f_{TJ})D_{TJ}} + \frac{f_{ig}f_{Bulk}(D_{ig}-D_{Bulk})^2}{f_{ig}(D_{ig}-D_{Bulk})-3D_{ig}}$$

where, f_{GB} f_{TJ}, f_{ig} are the volume fraction of GBs, TJs, and intergranular regions, respectively. The volume fraction parameters can be calculated with following equations,

$$f_{GB} = H_{GB}\frac{w}{d} = 2.9105\frac{w}{d}$$

$$f_{TJ} = H_{TJ}\left(\frac{w}{d}\right)^2 = 2.5259\left(\frac{w}{d}\right)^2$$

$$f_{ig} = f_{GB} + f_{TJ}$$

where H_{GB}, H_{TJ} are numerical factors determined by the grain shape and grain size distribution. D_{TJ}, D_{ig} are the diffusivity of triple junctions and intergranular regions (GBs and TJs). As D_{TJ} of Li is not available, assumptions are made that D_{TJ} could be 1, or 10^2, or 10^4 times that of D_{GB}. The equation for D_{ig} reads,

$$D_{ig} = \frac{1}{f_{ig}}\left[f_{GB}D_{GB} + f_{TJ}D_{TJ} + \frac{f_{TJ}f_{GB}(D_{TJ}-D_{GB})^2}{f_{TJ}(D_{TJ}-D_{GB})-2f_{ig}D_{TJ}}\right]$$

As shown in Figure S4, the prediction of the 2D grain model and the Maxwell-Garnet d' = 2,3 models are similar to those of the Hart model for grain sizes approximately larger than 100 nm. When D_{TJ} is assumed to be smaller than 10^2 D_{GB} (speculated to be reasonable guess given that D_{TJ} is approximately 2-10 times D_{GB} in Cu[6]), the model of Chen and Schuh is within the error-bar range of the Hart model except at the ~10^{-2} μm grain size. Given that various models for $D_{Polycrystal}$ predict comparable values and recent experimental reports have observed columnar shaped grains[7,8] in Li following plating, we adopted the Hart equation to predict the polycrystalline diffusivity of the Li anode in the current study.

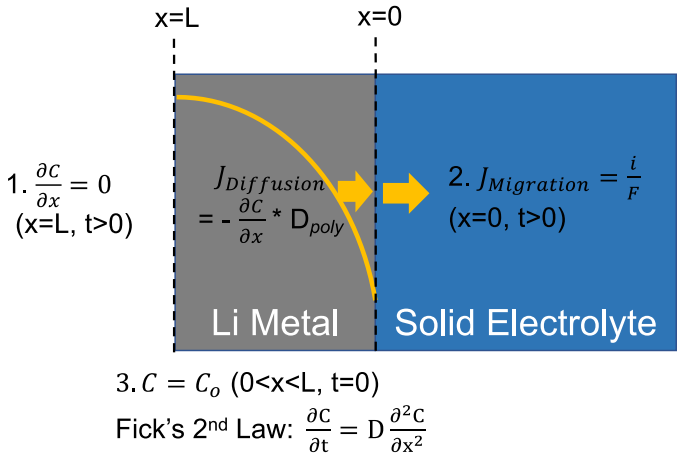

Figure S5. Boundary and initial conditions for the application of Fick's 2nd law to predict the Li concentration in the anode as a function of time and position. x=0 corresponds to the Li/SE interface, and x=L is an electrochemically non-active anode surface (corresponding to the current collector). The general solution is obtained under the following conditions:

1. There is no concentration gradient at x=L:

$$\frac{\partial C}{\partial x} = 0 \text{ (x=L, t>0).}$$

2. The Li flux, $J_{Migration}$, is driven by a constant current density i, at x=0

$$J_{Migration} = \frac{i}{F} \text{ (x=0, t>0).}$$

3. At t=0, the concentration of Li across the anode is constant everywhere and equal to $C_o = 0.078$ mol/cm^3:

$$C = C_o \text{ (0<x<L, t=0).}$$

The general solution with these boundary and initial conditions is given by:

$$C(x,t) = C_o - \frac{2It^{1/2}}{FD^{1/2}}\sum_{n=o}^{\infty}\left[ierfc\frac{2(n+1)L-x}{2(Dt)^{1/2}} + ierfc\frac{2nL+x}{2(Dt)^{1/2}}\right],$$

where t is time, x is position, D is the polycrystalline diffusivity, L is anode thickness, and F is Faraday's constant.

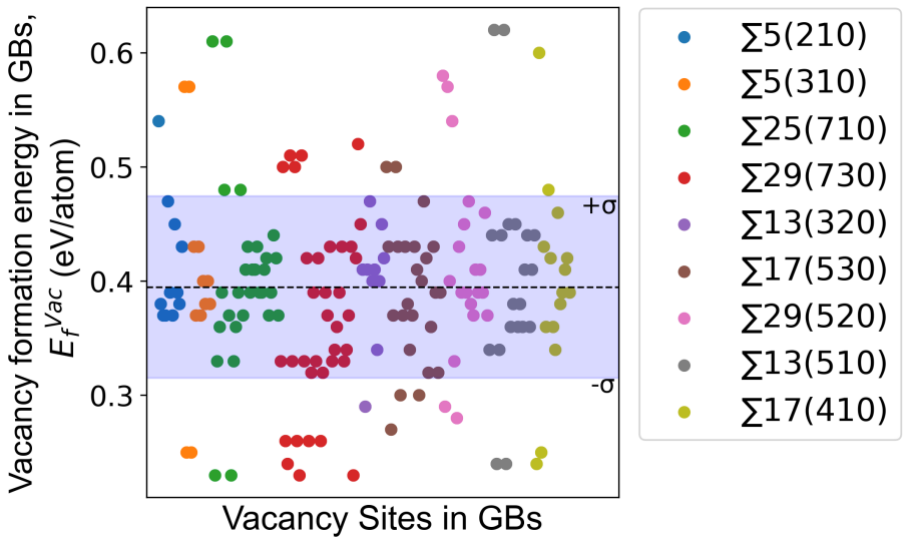

Figure S6. Vacancy formation energies (E_f^{vac}) measured at atomic sites in the structural unit of 9 subset tilt GB planes. A black dashed line and σ line show the average and standard deviation of E_f^{vac} of all datapoints, respectively. The bulk E_f^{vac} of Li is 0.4 eV/atom.

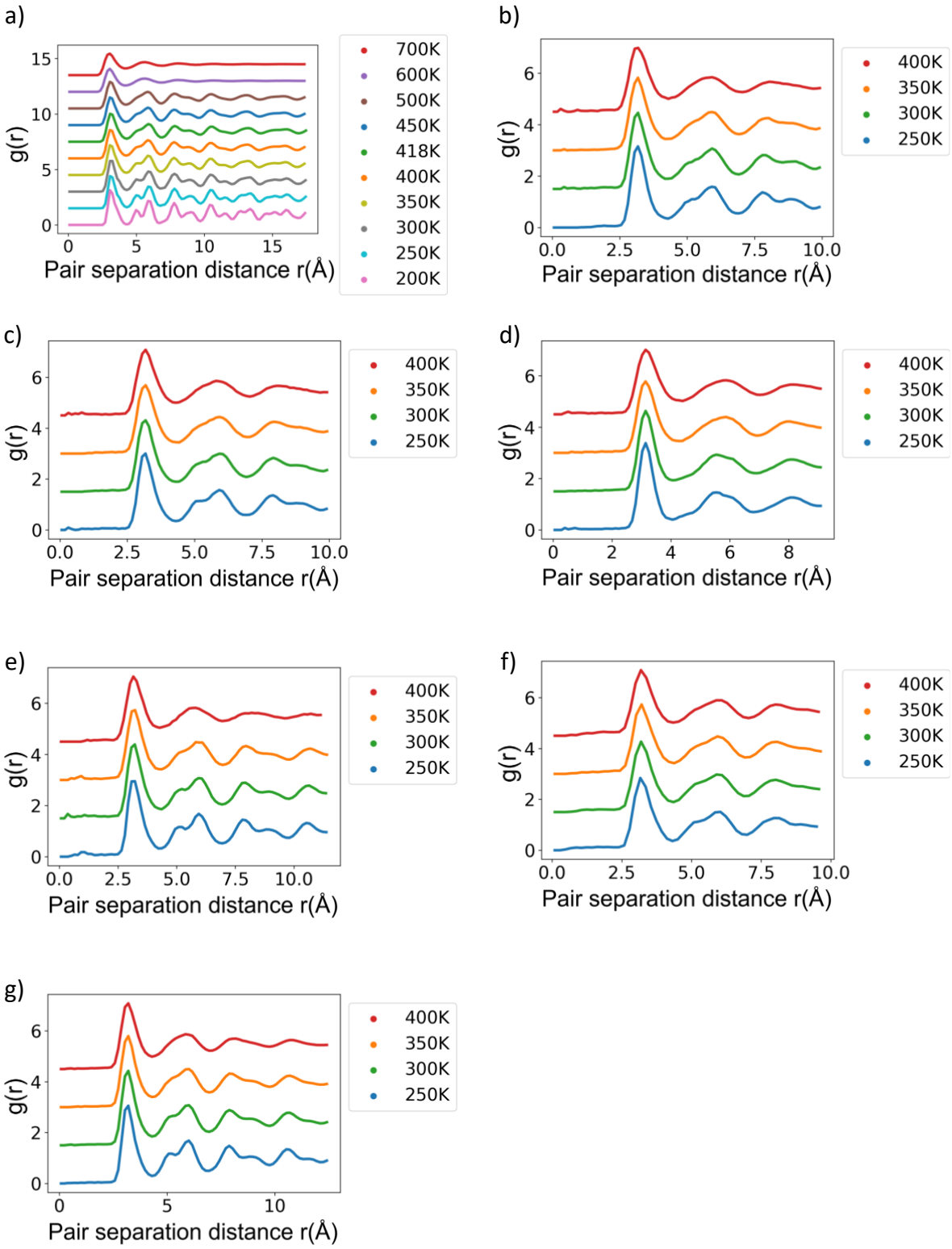

Figure S7. Pair distribution functions (PDFs) of 6 randomly chosen Li GBs compared to that of bulk Li. a) bulk Li, b) ∑5(210)/[001] tilt, c) ∑11(311)/[01-1] tilt, d) ∑31(156)/[11-1] tilt, e) ∑5(001)/53.13° twist, f) ∑11(01-1)/50.48° twist, and g) ∑13(11-1)/27.8° twist GBs. GB PDFs at 400 K are similar to that of melted bulk Li. (The melting temperature of the force field is 418 K.)

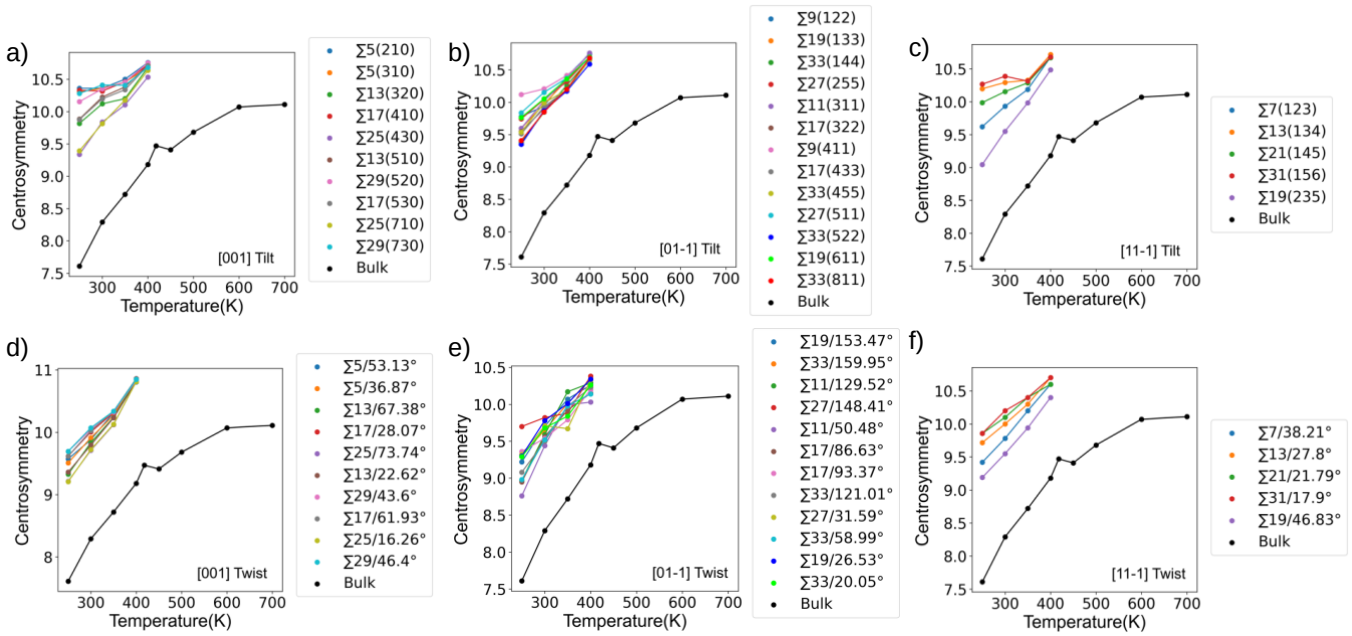

Figure S8. Calculated centrosymmetry parameter for 6 Li GBs: a) [001] tilt, b) [01-1] tilt, c) [11-1] tilt, d) [001] twist, e) [01-1] twist, and f) [11-1] twist rotation axes. For comparison, the centrosymmetry values for bulk Li is shown as the black line in each plot.

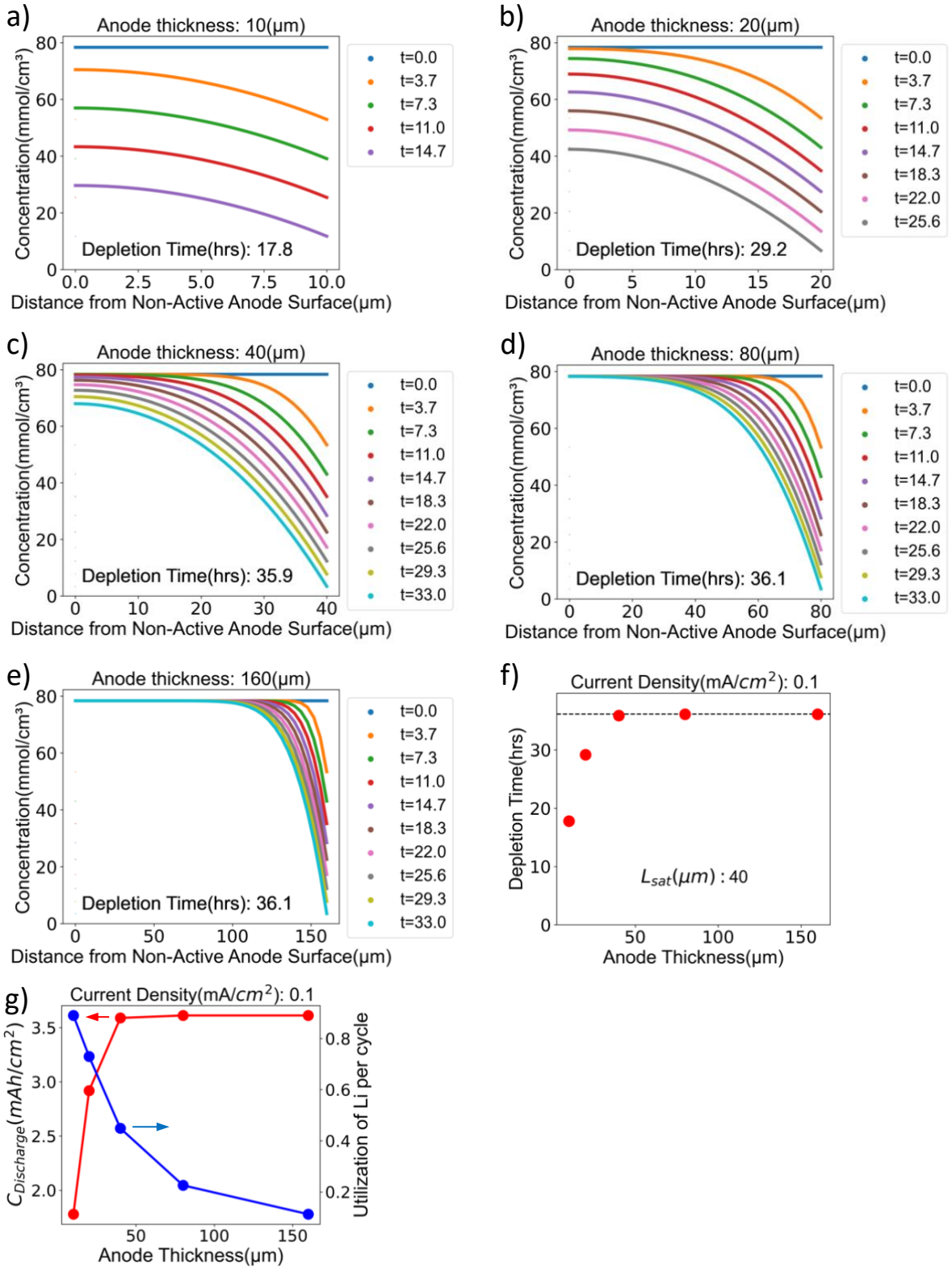

Figure S9. Concentration profiles for Li in the anode during discharge as a function of time and anode thickness. In panels a)-e) the current collector (the "Non-Active Anode Surface") is positioned at a distance of zero. The grain size is assumed to be 150 μm, with a stripping current density of 0.1mA/cm^2. Anode thickness include a) 10μm, b) 20μm, c) 40μm, d) 80μm, and e) 160μm. The depletion time as a function of anode thickness is plotted in f); the discharge capacity and Li utilization fraction as a function of anode thickness are plotted in g).

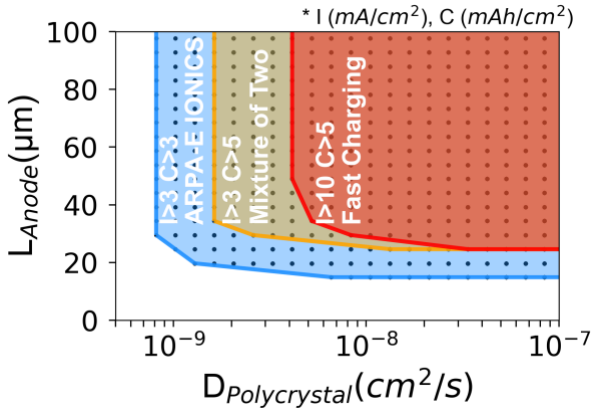

Figure S10. Design guidelines for Li metal anodes. Regions of different color indicate the combinations of polycrystalline self-diffusivity and anode thicknesses that satisfy three different battery performance goals for current density (I, mA/cm^2) and discharge capacity (C, mAh/cm^2).

Rotation Axis	GB plane	Misorientation Angle (°)	Simulation cell length			No. atoms in simulation cell
			Lx (Å)	Ly (Å)	Lz (Å)	
[001]	∑25(710)	16.26	98.63	98.63	13.95	12800
	∑13(510)	22.6	71.13	71.13	13.95	6528
	∑17(410)	28.07	57.51	71.89	13.95	5440
	∑5(310)	36.87	44.11	66.16	13.95	3776
	∑29(520)	43.6	75.12	75.12	13.95	7392
	∑29(730)	46.4	106.23	106.23	13.95	14720
	∑5(210)	53.13	31.19	77.98	13.95	3168
	∑17(530)	61.93	81.33	81.33	13.95	8640
	∑13(320)	67.38	50.29	75.44	13.95	4960
	∑25(430)	73.74	69.74	69.74	13.95	6396
[01-1]	∑33(811)	20.05	80.13	84.99	14.79	9360
	∑19(611)	26.53	60.8	64.49	14.79	5352
	∑27(511)	31.59	51.25	72.48	14.79	5136
	∑9(411)	38.94	41.85	73.97	14.79	4224
	∑11(311)	50.48	32.71	69.39	14.79	3120
	∑33(522)	58.99	56.66	60.1	14.79	4680
	∑3(211)	70.53	24.16	59.79	14.79	1968
	∑17(322)	86.63	40.67	71.89	14.79	3984
	∑17(433)	93.37	57.51	61	14.79	4776
	∑3(111)	109.47	34.17	60.4	14.79	2878
	∑33(455)	121.01	80.13	84.99	14.79	9495
	∑11(233)	129.52	46.26	65.43	14.79	4176
	∑9(122)	141.06	29.59	62.77	14.79	2600
	∑27(255)	148.41	72.48	76.88	14.79	7772
	∑19(133)	153.47	42.99	60.8	14.79	3648
	∑33(144)	159.95	56.66	60.1	14.79	4727
[11-1]	∑31(156)	17.9	95.12	82.37	18.12	13320
	∑21(145)	21.79	78.29	67.8	18.12	9000
	∑13(134)	27.8	61.6	71.13	18.12	7344
	∑7(123)	38.21	67.8	65.24	18.12	7452
	∑19(235)	46.83	74.47	64.49	18.12	8064

Table S1. Details for the symmetric tilt grain boundaries investigated in this study.

Rotation Axis	GB plane	Misorientation Angle (°)	Simulation cell length			No. of atoms in simulation cell
			Lx (Å)	Ly (Å)	Lz (Å)	
[001]	∑25(001)	16.26	49.32	62.77	49.32	14112
	∑13(001)	22.62	35.56	62.77	35.56	7344
	∑17(001)	28.07	43.13	62.77	43.13	10782
	∑5(001)	36.87	33.08	62.77	33.08	6336
	∑29(001)	43.6	37.56	62.77	37.56	8176
	∑29(001)	46.4	53.12	62.77	53.12	16352
	∑5(001)	53.13	23.39	62.77	23.39	3168
	∑17(001)	61.93	40.67	62.77	40.67	9584
	∑13(001)	67.38	37.72	62.77	37.72	8262
	∑25(001)	73.74	52.31	62.77	52.31	15876
[01-1]	∑33(01-1)	20.05	80.13	64.11	56.66	27456
	∑19(01-1)	26.53	60.8	64.11	42.99	15808
	∑27(01-1)	31.59	51.25	64.11	36.24	11232
	∑9(01-1)	38.94	41.85	64.11	29.59	7488
	∑11(01-1)	50.48	32.71	64.11	23.13	4560
	∑33(01-1)	58.99	56.66	64.11	40.06	13728
	∑3(01-1)	70.53	24.16	64.11	17.08	2496
	∑17(01-1)	86.63	40.67	64.11	28.76	7072
	∑17(01-1)	93.37	57.51	64.11	40.67	14144
	∑3(01-1)	109.47	25.63	64.11	18.12	2808
	∑33(01-1)	121.01	80.13	64.11	56.66	27456
	∑11(01-1)	129.52	46.26	64.11	32.71	9120
	∑9(01-1)	141.06	44.38	64.11	31.38	8424
	∑27(01-1)	148.41	72.48	64.11	51.25	22464
	∑19(01-1)	153.47	42.99	64.11	30.4	7904
	∑33(01-1)	159.95	56.66	64.11	40.06	13728
[11-1]	∑31(11-1)	17.9	95.12	60.4	54.92	29160
	∑21(11-1)	21.79	78.29	60.4	45.2	19821
	∑13(11-1)	27.8	61.6	60.4	35.56	12293
	∑7(11-1)	38.21	67.8	60.4	39.14	14936
	∑19(11-1)	46.83	74.47	60.4	42.99	18032

Table S2. Structural parameters for twist grain boundaries investigated in this study.

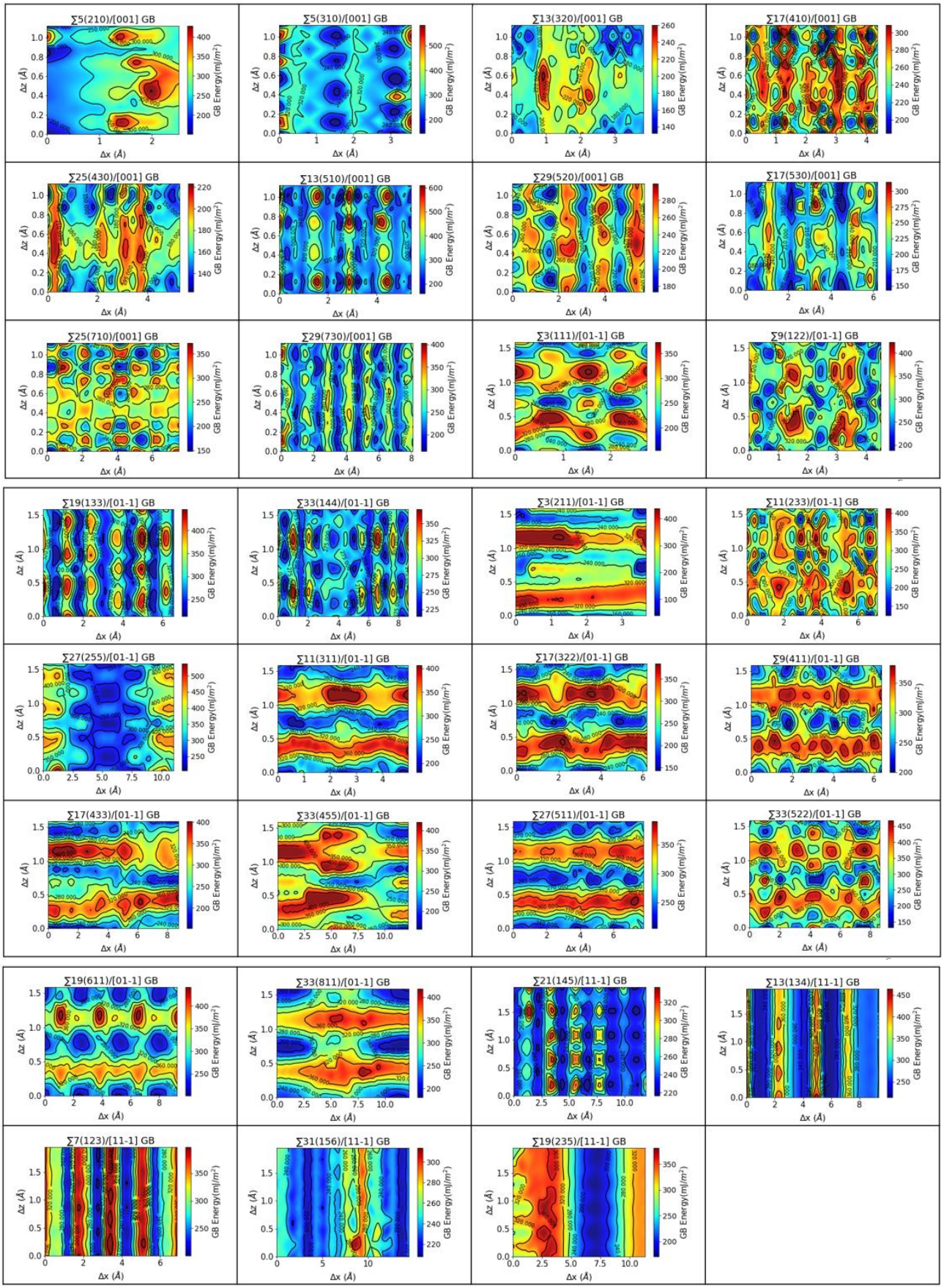

Table S3. Calculated γ surfaces for symmetric tilt grain boundaries.

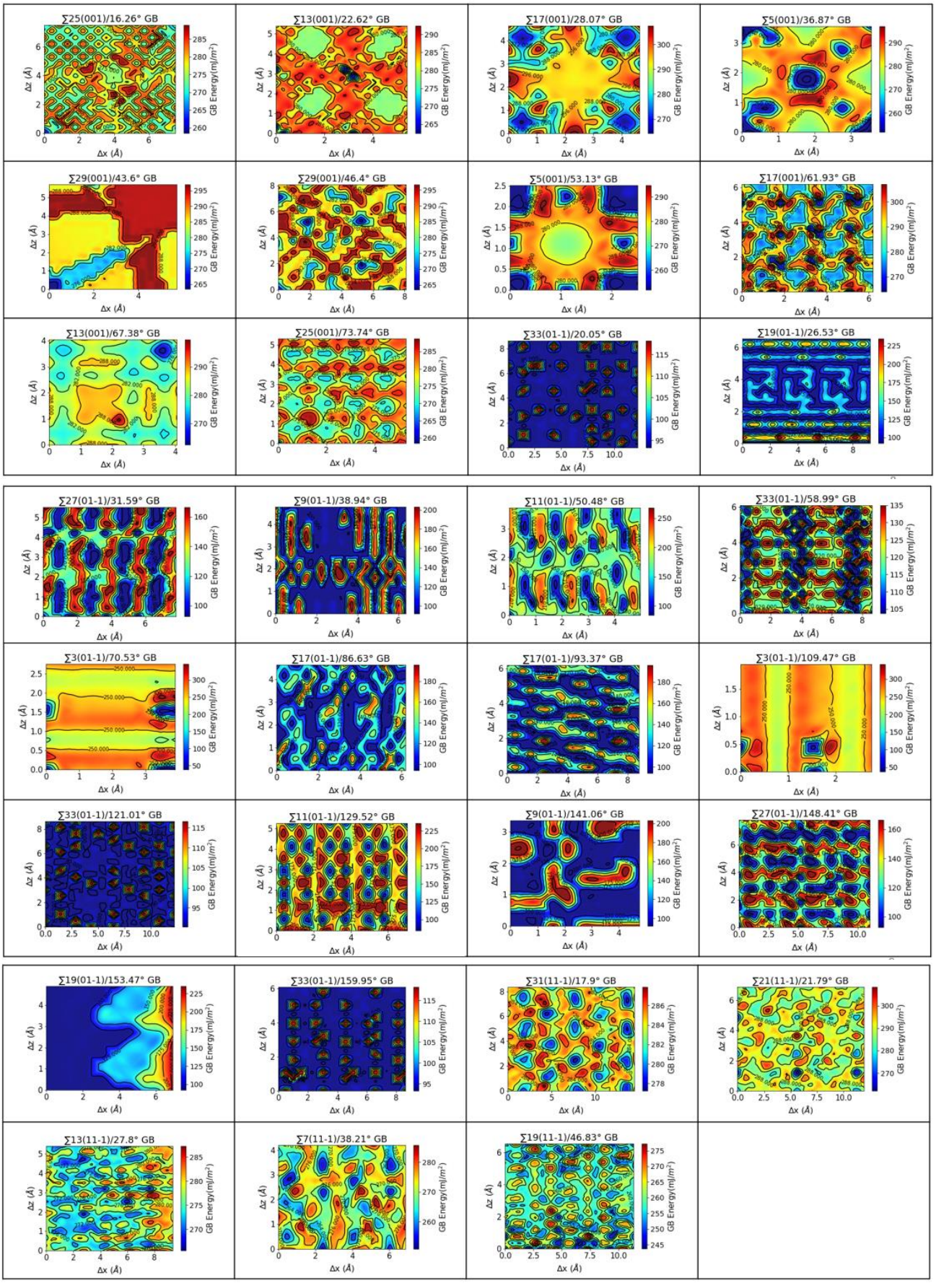

Table S4. Calculated γ surfaces for twist grain boundaries.

a) [001] tilt\Temperature (K)	250	300	350	400
∑5(210)	7.2	7.8	9.5	16.2
∑5(310)	8.2	8.5	11.4	18.1
∑13(320)	8.9	9.6	10.9	13.5
∑17(410)	8.1	9.3	11.6	16.3
∑25(430)	10.2	9.5	10.2	12.7
∑13(510)	8.9	9.3	11	15
∑29(520)	8.8	9.1	12.6	18.9
∑17(530)	8.9	9.4	10.5	18.4
∑25(710)	10.8	11.2	12.6	14.3
∑29(730)	8.3	9	13.6	19.8
b) [01-1] tilt\Temperature (K)	250	300	350	400
∑9(122)	12.7	14.3	12.5	15.6
∑19(133)	13	13.2	13.6	17
∑33(144)	13.7	14.1	13.5	16.3
∑27(255)	11.8	12.7	14.2	18
∑11(311)	14.8	12.7	13.3	15.9
∑17(322)	13.2	13.3	13.1	13.7
∑9(411)	6.6	7	13	17
∑17(433)	16	14.1	14.5	16.2
∑33(455)	17.1	14.9	14.3	14.9
∑27(511)	8.7	11.5	14.2	17
∑33(522)	13	13	12.9	13.4
∑19(611)	11.6	12.5	14.4	17.6
∑33(811)	12.1	12.3	13.2	16.2
c) [11-1] tilt\Temperature (K)	250	300	350	400
∑7(123)	12.7	12.7	13.4	16.6
∑13(134)	12.3	13.1	12.6	16.6
∑21(145)	11.8	12.6	12.8	17.7
∑31(156)	10.7	10.9	12.9	17.1
∑19(235)	13.4	14.4	13.4	14.4
d) [001] twist\Temperature (K)	250	300	350	400
∑5(001)/53.13°	14.7	15.3	15.4	17.0
∑5(001)/36.87°	15.2	15.5	15.5	18.9
∑13(001)/67.38°	15.5	15.3	15.2	18.0
∑17(001)/28.07°	14.2	14.3	14.9	19.8
∑25(001)/73.74°	16.6	15.9	16.1	16.9
∑13(001)/22.62°	15.4	15.4	15.2	17.4
∑29(001)/43.6°	14.5	14.8	15.6	20.2
∑17(001)/61.93°	13.7	14.0	14.6	19.2
∑25(001)/16.26°	16.2	15.5	15.6	17.2
∑29(001)/46.4°	14.6	14.8	15.3	21.8

e) [01-1] twist\Temperature (K)	250	300	350	400
∑19(01-1)/153.47°	6.6	6.8	7.2	9.1
∑33(01-1)/159.95°	6.5	6.7	7.2	9.4
∑11(01-1)/129.52°	8.8	8.7	8.3	11.2
∑27(01-1)/148.41°	6.8	7.4	8.0	9.7
∑11(01-1)/50.48°	7.6	7.9	7.9	9.3
∑17(01-1)/86.63°	5.9	6.3	6.6	8.7
∑17(01-1)/93.37°	6.2	6.8	7.2	7.9
∑33(01-1)/121.01°	9.3	10.0	9.8	12.2
∑27(01-1)/31.59°	7.3	7.6	7.7	9.4
∑33(01-1)/58.99°	7.8	8.1	8.3	9.8
∑19(01-1)/26.53°	6.5	6.9	7.7	8.8
∑33(01-1)/20.05°	6.7	6.9	7.3	9.0
f) [11-1] twist\Temperature (K)	250	300	350	400
∑7(11-1)/38.21°	10.7	10.9	11.2	14.4
∑13(11-1)/27.8°	9.9	10.3	11.4	19.7
∑21(11-1)/21.79°	9.8	10.6	12.6	17.9
∑31(11-1)/17.9°	10.8	11.4	12.5	20.4
∑19(11-1)/46.83°	10.1	11.3	11.9	14.7
g) Average GB width\Temperature (K)	250	300	350	400
	10.9	11.2	12	15.3

Table S5. Calculated GB widths (Å) of (a)-(c) tilt GBs, (d)-(f) twist GBs, and (g) the average across all GBs as a function of temperature. The value at each temperature is sampled every 0.1 ns and time-averaged.

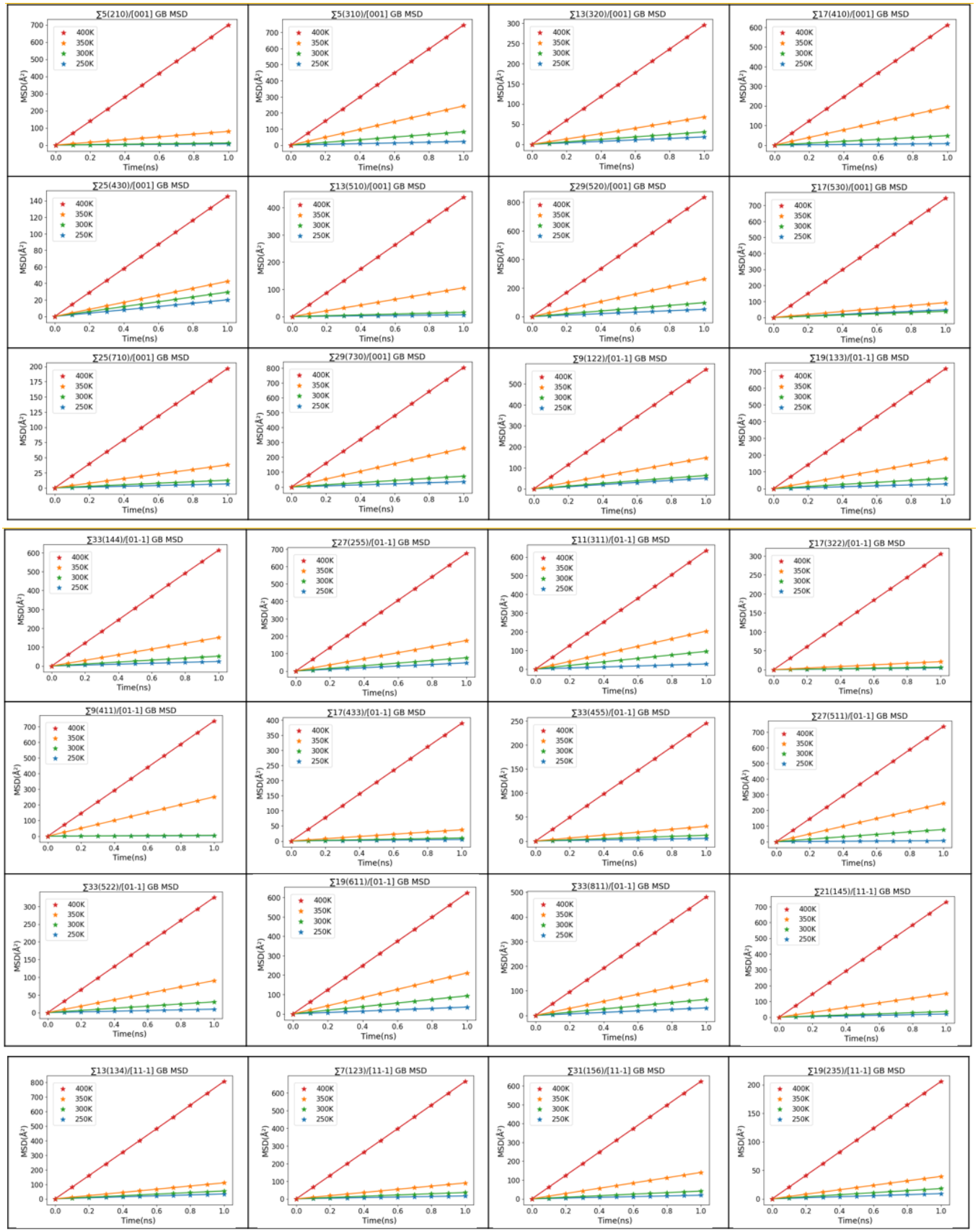

Table S6. Calculated mean squared displacements for diffusion in symmetric tilt GBs.

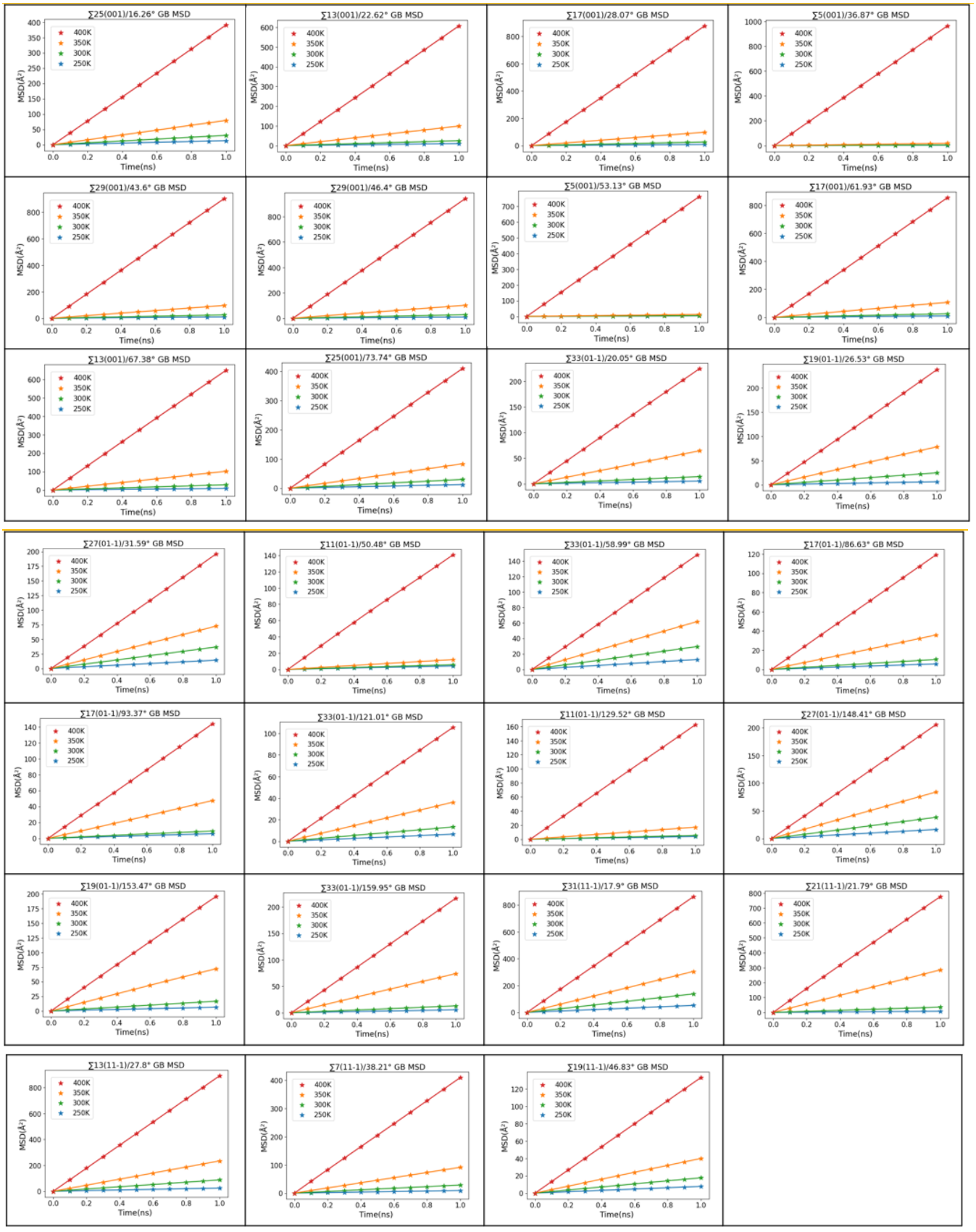

Table S7. Calculated mean squared displacements for diffusion in twist GBs.

	Fit to 250, 300, and 350 K			Fit to 300, 350, and 400 K		
Tilt GB	**E_a (eV)**	**D_0 (cm^2/s)**	**R^2**	**E_a (eV)**	**D_0 (cm^2/s)**	**R^2**
∑5(210)	0.18	$3.66*10^{-4}$	0.83	0.41	1.28	0.96
∑5(310)	0.18	$1.72E*10^{-3}$	0.99	0.23	$8.77*10^{-3}$	0.99
∑13(320)	0.1	$2.40*10^{-5}$	0.95	0.23	$2.80*10^{-3}$	0.92
∑17(410)	0.25	$1.25*10^{-2}$	1	0.27	$2.39*10^{-2}$	1
∑25(430)	0.07	$6.95*10^{-6}$	0.96	0.16	$2.49*10^{-4}$	0.92
∑13(510)	0.2	$1.17*10^{-3}$	0.88	0.34	$1.38*10^{-1}$	1
∑29(520)	0.13	$2.71*10^{-4}$	0.96	0.22	$6.93*10^{-3}$	0.97
∑17(530)	0.05	$6.36*10^{-6}$	0.61	0.3	$5.41*10^{-2}$	0.86
∑25(710)	0.13	$4.14*10^{-5}$	0.93	0.28	$1.06*10^{-2}$	0.94
∑29(730)	0.16	$6.78*10^{-4}$	0.95	0.24	$1.48*10^{-2}$	0.99
∑9(122)	0.09	$3.64*10^{-5}$	0.89	0.22	$5.33*10^{-3}$	0.94
∑19(133)	0.14	$2.40*10^{-4}$	0.95	0.25	$1.55*10^{-2}$	0.96
∑33(144)	0.13	$1.89*10^{-4}$	0.96	0.25	$1.47*10^{-2}$	0.95
∑27(255)	0.1	$6.85*10^{-5}$	0.94	0.22	$6.44*10^{-3}$	0.93
∑11(311)	0.15	$5.36*10^{-4}$	1	0.19	$2.58*10^{-3}$	0.96
∑17(322)	0.11	$1.09*10^{-5}$	0.87	0.38	$1.92*10^{-1}$	0.82
∑9(411)	0.3	$3.87*10^{-2}$	0.5	0.53	$7.51*10^{1}$	0.44
∑17(433)	0.14	$6.04*10^{-5}$	0.89	0.38	$2.60*10^{-1}$	0.89
∑33(455)	0.12	$2.67*10^{-5}$	0.97	0.3	$2.08*10^{-2}$	0.86
∑27(511)	0.28	$4.93*10^{-2}$	0.94	0.23	$8.86*10^{-3}$	0.99
∑33(522)	0.17	$3.72*10^{-4}$	0.99	0.24	$5.09*10^{-3}$	0.98
∑19(611)	0.13	$2.92*10^{-4}$	1	0.2	$2.73*10^{-3}$	0.97
∑33(811)	0.12	$1.10*10^{-4}$	0.99	0.2	$2.40*10^{-3}$	0.95
∑7(123)	0.12	$6.05*10^{-5}$	0.96	0.29	$4.12*10^{-2}$	0.86
∑13(134)	0.09	$3.10*10^{-5}$	0.93	0.27	$2.75*10^{-2}$	0.86
∑21(145)	0.14	$2.12*10^{-4}$	0.88	0.31	$8.16*10^{-2}$	0.97
∑31(156)	0.15	$2.47*10^{-4}$	0.92	0.28	$3.20*10^{-2}$	0.97
∑19(235)	0.11	$1.96*10^{-5}$	0.96	0.25	$4.30*10^{-3}$	0.89
Bulk(cal)	0.48	$2.18*10^{-3}$	1	0.48		1

Table S8. Arrhenius parameters for tilt GBs calculated using fits to low temperature data (250K, 300K, 350K) and high temperature data (300K, 350K, 400K). The calculated values for diffusion in the bulk via a vacancy mechanism are presented for comparison.

	Fit to 250, 300, and 350 K			Fit to 300, 350, and 400 K		
Twist GB	**E_a (eV)**	**D_0 (cm^2/s)**	**R^2**	**E_a (eV)**	**D_0 (cm^2/s)**	**R^2**
∑5(001)/53.13°	0.1	$5.71*10^{-6}$	0.83	0.51	1.75*10	0.63
∑5(001)/36.87°	0.12	$1.24*10^{-5}$	0.82	0.53	4.23*10	0.66
∑13(001)/67.38°	0.18	$7.33*10^{-4}$	0.97	0.32	$1.02*10^{-1}$	0.94
∑17(001)/28.07°	0.18	$6.49*10^{-4}$	0.96	0.36	$3.44*10^{-1}$	0.92
∑25(001)/73.74°	0.14	$1.25*10^{-4}$	0.97	0.26	$1.05*10^{-2}$	0.93
∑13(001)/22.62°	0.17	$3.64*10^{-4}$	0.93	0.33	$1.13*10^{-1}$	0.95
∑29(001)/43.6°	0.17	$4.33*10^{-4}$	0.96	0.36	$3.93*10^{-1}$	0.9
∑17(001)/61.93°	0.18	$5.35*10^{-4}$	0.95	0.36	$3.48*10^{-1}$	0.92
∑25(001)/16.26°	0.14	$1.12*10^{-4}$	0.98	0.26	$1.01*10^{-2}$	0.93
∑29(001)/46.4°	0.18	$5.54*10^{-4}$	0.96	0.36	$4.47*10^{-1}$	0.9
∑19(01-1)/153.47°	0.17	$3.36*10^{-4}$	0.94	0.25	$4.77*10^{-3}$	1
∑33(01-1)/159.95°	0.18	$3.63*10^{-4}$	0.89	0.29	$1.83*10^{-2}$	1
∑11(01-1)/129.52°	0.11	$7.44*10^{-6}$	0.83	0.35	$5.07*10^{-2}$	0.88
∑27(01-1)/148.41°	0.12	$7.55*10^{-5}$	1	0.17	$3.74*10^{-4}$	0.97
∑11(01-1)/50.48°	0.07	$1.81*10^{-6}$	0.88	0.32	$1.70*10^{-2}$	0.79
∑17(01-1)/86.63°	0.14	$4.30*10^{-5}$	0.9	0.27	$4.56*10^{-3}$	0.98
∑17(01-1)/93.37°	0.15	$7.96*10^{-5}$	0.86	0.29	$1.11*10^{-2}$	1
∑33(01-1)/121.01°	0.13	$3.53*10^{-5}$	0.95	0.21	$7.74*10^{-4}$	0.99
∑27(01-1)/31.59°	0.12	$7.27*10^{-5}$	1	0.17	$3.99*10^{-4}$	0.97
∑33(01-1)/58.99°	0.11	$4.28*10^{-5}$	0.99	0.17	$3.26*10^{-4}$	0.98
∑19(01-1)/26.53°	0.19	$6.06*10^{-4}$	0.99	0.23	$3.07*10^{-3}$	1
∑33(01-1)/20.05°	0.18	$3.59*10^{-4}$	0.92	0.29	$1.50*10^{-2}$	1
∑7(11-1)/38.21°	0.18	$5.13*10^{-4}$	0.98	0.27	$1.60*10^{-2}$	0.97
∑13(11-1)/27.8°	0.17	$9.03*10^{-4}$	1	0.23	$1.15*10^{-2}$	0.95
∑21(11-1)/21.79°	0.28	$4.75*10^{-2}$	0.99	0.24	$1.50*10^{-2}$	1
∑31(11-1)/17.9°	0.13	$4.26*10^{-4}$	1	0.19	$2.96*10^{-3}$	0.97
∑19(11-1)/46.83°	0.12	$3.53*10^{-5}$	0.99	0.2	$6.30*10^{-4}$	0.95
Bulk(cal)	0.48	$2.18*10^{-3}$	1	0.48	$2.18*10^{-3}$	1

Table S9. Arrhenius parameters for twist GBs calculated using fits to low temperature data (250K, 300K, 350K) and high temperature data (300K, 350K, 400K). The calculated values for diffusion in the bulk via a vacancy mechanism are presented for comparison.

GB System	Diffusivity without added vacancies (cm^2/s)	Diffusivity with added vacancies (cm^2/s)
∑5(210)	$2.2*10^{-7}$	$4.6*10^{-7}$
∑5(310)	$1.3*10^{-6}$	$1.3*10^{-6}$
∑13(320)	$5.1*10^{-7}$	$6.9*10^{-7}$
∑17(530)	$6.2*10^{-7}$	$3.3*10^{-7}$
∑25(710)	$2.1*10^{-7}$	$2.1*10^{-7}$
∑29(730)	$1.2*10^{-6}$	$1.3*10^{-6}$

Table S10. GB Diffusivity with and without added GB vacancies at 300 K.

Temperature(K)	250	300	350	400
D_Tot	$2.6*10^{-7}$	$6.2*10^{-7}$	$1.9*10^{-6}$	$8.5*10^{-6}$
D_X	$1.8*10^{-7}$	$5.4*10^{-7}$	$1.9*10^{-6}$	$9.4*10^{-6}$
D_Y	$1.4*10^{-7}$	$3.5*10^{-7}$	$1.2*10^{-6}$	$5.9*10^{-6}$
D_Z	$4.7*10^{-7}$	$9.7*10^{-7}$	$2.5*10^{-6}$	$1.0*10^{-5}$

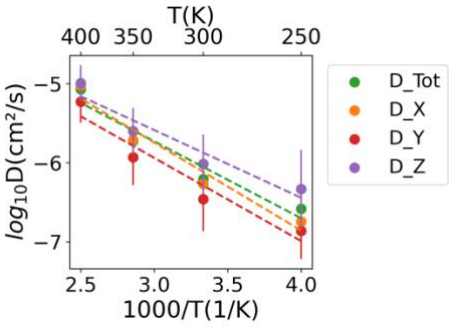

Table S11. Total and directionally-resolved GB diffusivity (cm^2/s) averaged over all GBs. D_Y is the diffusivity resolved along the direction perpendicular to the GB planes (i.e., y direction) and D_X and D_Z are the diffusivities within the GB planes (i.e., x and z directions). The right figure plots the average diffusivities in an Arrhenius plot.

Tilt GB	D_Tot (cm^2/s)	D_X (cm^2/s)	D_Y (cm^2/s)	D_Z (cm^2/s)
∑5(210)	$2.2*10^{-7}$	$1.3*10^{-7}$	$1.4*10^{-7}$	$3.9*10^{-7}$
∑5(310)	$1.3*10^{-6}$	$1.0*10^{-6}$	$7.0*10^{-7}$	$2.2*10^{-6}$
∑13(320)	$5.1*10^{-7}$	$1.9*10^{-7}$	$9.8*10^{-8}$	$1.2*10^{-6}$
∑17(410)	$7.9*10^{-7}$	$7.0*10^{-7}$	$5.9*10^{-7}$	$1.1*10^{-6}$
∑25(430)	$4.9*10^{-7}$	$2.0*10^{-7}$	$1.5*10^{-7}$	$1.1*10^{-6}$
∑13(510)	$2.7*10^{-7}$	$2.6*10^{-7}$	$2.4*10^{-7}$	$3.2*10^{-7}$
∑29(520)	$1.7*10^{-6}$	$1.0*10^{-6}$	$6.3*10^{-7}$	$3.3*10^{-6}$
∑17(530)	$6.2*10^{-7}$	$1.5*10^{-7}$	$1.6*10^{-7}$	$1.5*10^{-6}$
∑25(710)	$2.1*10^{-7}$	$2.0*10^{-7}$	$2.0*10^{-7}$	$2.2*10^{-7}$
∑29(730)	$1.2*10^{-6}$	$7.0*10^{-7}$	$5.3*10^{-7}$	$2.5*10^{-6}$
∑9(122)	$1.0*10^{-6}$	$5.6*10^{-7}$	$3.4*10^{-7}$	$2.2*10^{-6}$
∑19(133)	$1.0*10^{-6}$	$8.5*10^{-7}$	$5.9*10^{-7}$	$1.6*10^{-6}$
∑33(144)	$8.7*10^{-7}$	$7.3*10^{-7}$	$5.7*10^{-7}$	$1.3*10^{-6}$
∑27(255)	$1.3*10^{-6}$	$1.1*10^{-6}$	$6.1*10^{-7}$	$2.1*10^{-6}$
∑11(311)	$1.5*10^{-6}$	$2.1*10^{-6}$	$1.0*10^{-6}$	$1.5*10^{-6}$
∑17(322)	$1.1*10^{-7}$	$1.3*10^{-7}$	$1.1*10^{-7}$	$1.0*10^{-7}$
∑9(411)	$8.3*10^{-8}$	$8.8*10^{-8}$	$7.4*10^{-8}$	$8.8*10^{-8}$
∑17(433)	$1.6*10^{-7}$	$1.4*10^{-7}$	$1.7*10^{-7}$	$1.5*10^{-7}$
∑33(455)	$2.0*10^{-7}$	$1.5*10^{-7}$	$2.4*10^{-7}$	$2.0*10^{-7}$
∑27(511)	$1.3*10^{-6}$	$1.2*10^{-6}$	$1.1*10^{-6}$	$1.7*10^{-6}$
∑33(522)	$4.9*10^{-7}$	$5.9*10^{-7}$	$3.1*10^{-7}$	$5.8*10^{-7}$
∑19(611)	$1.5*10^{-6}$	$1.3*10^{-6}$	$1.4*10^{-6}$	$2.0*10^{-6}$
∑33(811)	$1.1*10^{-6}$	$4.0*10^{-7}$	$1.0*10^{-6}$	$1.9*10^{-6}$
∑7(123)	$5.9*10^{-7}$	$9.2*10^{-8}$	$1.3*10^{-7}$	$1.6*10^{-6}$
∑13(134)	$8.6*10^{-7}$	$8.8*10^{-8}$	$8.4*10^{-8}$	$2.4*10^{-6}$
∑21(145)	$5.8*10^{-7}$	$8.7*10^{-8}$	$8.2*10^{-8}$	$1.6*10^{-6}$
∑31(156)	$6.6*10^{-7}$	$1.0*10^{-7}$	$8.0*10^{-8}$	$1.8*10^{-6}$
∑19(235)	$2.8*10^{-7}$	$8.5*10^{-8}$	$1.4*10^{-7}$	$6.1*10^{-7}$

Table S12. Calculated GB diffusivity in tilt GBs at 300 K resolved normal to the GB plane (y direction) and within the GB plane (x and z directions). D_Tot represents the GB diffusivity averaged in x, y, and z.

Twist GB	D_Tot (cm^2/s)	D_X (cm^2/s)	D_Y (cm^2/s)	D_Z (cm^2/s)
∑5(001)/53.13°	$8.0*10^{-8}$	$7.9*10^{-8}$	$8.0*10^{-8}$	$8.0*10^{-8}$
∑5(001)/36.87°	$7.9*10^{-8}$	$7.9*10^{-8}$	$8.2*10^{-8}$	$7.7*10^{-8}$
∑13(001)/67.38°	$4.8*10^{-7}$	$5.4*10^{-7}$	$4.1*10^{-7}$	$4.9*10^{-7}$
∑17(001)/28.07°	$4.3*10^{-7}$	$4.6*10^{-7}$	$3.8*10^{-7}$	$4.6*10^{-7}$
∑25(001)/73.74°	$5.1*10^{-7}$	$5.3*10^{-7}$	$4.6*10^{-7}$	$5.3*10^{-7}$
∑13(001)/22.62°	$4.1*10^{-7}$	$4.4*10^{-7}$	$3.5*10^{-7}$	$4.4*10^{-7}$
∑29(001)/43.6°	$4.4*10^{-7}$	$4.6*10^{-7}$	$4.0*10^{-7}$	$4.5*10^{-7}$
∑17(001)/61.93°	$4.4*10^{-7}$	$4.7*10^{-7}$	$3.8*10^{-7}$	$4.7*10^{-7}$
∑25(001)/16.26°	$5.1*10^{-7}$	$5.4*10^{-7}$	$4.6*10^{-7}$	$5.3*10^{-7}$
∑29(001)/46.4°	$4.5*10^{-7}$	$4.7*10^{-7}$	$4.1*10^{-7}$	$4.7*10^{-7}$
∑19(01-1)/153.47°	$3.0*10^{-7}$	$3.5*10^{-7}$	$1.0*10^{-7}$	$4.5*10^{-7}$
∑33(01-1)/159.95°	$2.1*10^{-7}$	$2.2*10^{-7}$	$9.4*10^{-8}$	$3.2*10^{-7}$
∑11(01-1)/129.52°	$8.5*10^{-8}$	$8.9*10^{-8}$	$6.5*10^{-8}$	$1.0*10^{-7}$
∑27(01-1)/148.41°	$6.6*10^{-7}$	$9.8*10^{-7}$	$1.7*10^{-7}$	$8.3*10^{-7}$
∑11(01-1)/50.48°	$8.9*10^{-8}$	$1.1*10^{-7}$	$6.2*10^{-8}$	$9.5*10^{-8}$
∑17(01-1)/86.63°	$1.6*10^{-7}$	$2.0*10^{-7}$	$7.2*10^{-8}$	$2.0*10^{-7}$
∑17(01-1)/93.37°	$1.5*10^{-7}$	$1.8*10^{-7}$	$7.6*10^{-8}$	$2.1*10^{-7}$
∑33(01-1)/121.01°	$2.2*10^{-7}$	$2.4*10^{-7}$	$7.8*10^{-8}$	$3.4*10^{-7}$
∑27(01-1)/31.59°	$6.0*10^{-7}$	$7.8*10^{-7}$	$1.5*10^{-7}$	$8.8*10^{-7}$
∑33(01-1)/58.99°	$4.9*10^{-7}$	$8.1*10^{-7}$	$9.4*10^{-8}$	$5.6*10^{-7}$
∑19(01-1)/26.53°	$4.0*10^{-7}$	$5.6*10^{-7}$	$1.3*10^{-7}$	$5.0*10^{-7}$
∑33(01-1)/20.05°	$2.3*10^{-7}$	$3.3*10^{-7}$	$1.0*10^{-7}$	$2.5*10^{-7}$
∑7(11-1)/38.21°	$4.8*10^{-7}$	$5.9*10^{-7}$	$2.6*10^{-7}$	$5.8*10^{-7}$
∑13(11-1)/27.8°	$1.5*10^{-6}$	$1.8*10^{-6}$	$7.5*10^{-7}$	$1.8*10^{-6}$
∑21(11-1)/21.79°	$1.0*10^{-6}$	$1.0*10^{-6}$	$5.0*10^{-7}$	$1.5*10^{-6}$
∑31(11-1)/17.9°	$2.3*10^{-6}$	$2.8*10^{-6}$	$1.3*10^{-6}$	$2.8*10^{-6}$
∑19(11-1)/46.83°	$3.0*10^{-7}$	$3.6*10^{-7}$	$1.8*10^{-7}$	$3.5*10^{-7}$

Table S13. Calculated GB diffusivity in twist GBs at 300 K resolved normal to the GB plane (y direction) and within the GB plane (x and z directions). D_Tot represents the GB diffusivity averaged in x, y, and z.

Notes and references

1 E. W. Hart, *Acta metallurgica 5.10 (1957): 597.*

2 I. V. Belova and G. E. Murch, *Journal of Physics and Chemistry of Solids*, 2003, **64**, 873–878.

3 J.C. Maxwell-Garnett, *Philos. Trans. R. Soc. London*, 1904, **203**, 385–420.

4 J. R. Kalnin and E. Kotomin, *J Phys A Math Gen*, 1998, **31**, 7227–7234.

5 Y. Chen and C. A. Schuh, *J Appl Phys*, 2007, **101**, 063524.

6 T. Frolov and Y. Mishin, *Phys Rev B Condens Matter Mater Phys*, 2009, **79**, 174110.

7 M. Motoyama, M. Ejiri and Y. Iriyama, *J Electrochem Soc*, 2015, **162**, A7067–A7071.

8 M. A. Citrin, H. Yang, S. K. Nieh, J. Berry, W. Gao, X. Pan, D. J. Srolovitz and J. R. Greer, *MRS Bull*, 2020, **45**, 891–904.